Journal of King Saud University – Science 31 (2019) 1122–1126

Contents lists available at ScienceDirect

Journal of King Saud University – Science

journal homepage: www.sciencedirect.com

Effect of silicon carbide addition on the microstructure, hardness and densification properties of spark plasma sintered Ni-Zn-Al alloy

Katlego M. Mampuru [a], Emmanuel Ajenifuja [a,b,*], A.P.I. Popoola [a], Olawale Popoola [b]

[a] Department of Chemical, Metallurgical and Materials Engineering, Tshwane University of Technology, Pretoria West, Pretoria 0183, South Africa
[b] Center for Energy and Electric Power, Tshwane University of Technology, Pretoria, South Africa

ARTICLE INFO

Article history:
Received 15 July 2018
Accepted 17 January 2019
Available online 19 January 2019

Keywords:
Nickel
Silicon carbide
Spark plasma sintering
Microstructure
Microhardness

ABSTRACT

Effect of silicon carbide (SiC) additions on the physico-chemical properties of nickel-zinc-aluminium (Ni-Zn-Al) alloy prepared by spark plasma sintering technique is investigated. Elemental powder matrix samples were prepared with different amounts of SiC (1–4 wt%) and were mixed in a tubular mixer for 5 h at 49 rpm. The metal-ceramic composite powders were pressed and sintered at 850 °C with 100 °C/min heating rates, 10 min holding time and a pressure of 50 MPa. Hard disk-shaped metal matrix composite pellets (⌀ = 40 mm, thickness = 5 mm) were obtained. Chemical, physical and microstructural properties of sintered composite samples were studied. The results show that SiC addition particles influence the physical and microstructural characteristics metal matrix composites. The samples demonstrated significant increase in relative density (83–96.53%) and hardness (132–228.36 HV) with increase in SiC additions. Compositional analysis indicated predominant nickel and silicon carbide in identified phases.

1. Introduction

One of the challenges encountered in advancing solid oxide fuel cell (SOFC) technology is the development of interconnect materials with adequate conductivity and stability for efficient long-term use. The progress in the fabrication technology of SOFCs has made it possible to reduce the cell operating temperature from 1000 °C to the intermediate 600–800 °C without compromising its performance (Charpentier, 2000; Wachsman and Lee, 2011). The lower operating temperatures enable the use of high temperature oxidation resistant metal-based interconnects in place of their ceramic counterparts. Interconnects should be materials with good resistance against oxidation, low electrical resistivity of oxide scale, comparable thermal expansion and adequate mechanical strength (Linderoth, 1996). Thus, the metallic interconnects offer many advantages over their ceramic counterpart in terms of availability, stability, electrical conductivity, thermal conductivity, ease of manufacturing and low cost. However, the formation of a chromia subscale during operation causes serious problems (Folgner, 2017). Ceramic-metal composites are already under consideration as interconnect in solid oxide fuel cell architecture, as they have shown resilience in thermal stability and electrical conductivity. Nickel alloys, due to their unique mechanical and thermal properties are of high consideration as interconnect. Besides, nickel alloys have an added advantage of exhibiting better corrosion behaviour which is attributed to passive film formation on its surface. The applications of nickel and its alloys can be found in almost every engineering field such as aerospace, marine, automotive, structural and various other fields (Borkar and Banerjee, 2014; Tang et al., 2009), due to its favourable properties such as high specific strength, high corrosion, fatigue resistance and toughness (Mohanta et al., 2014; Zeblon et al., 2018). Meanwhile, nickel-based metal matrix composites are preferred in numerous applications with crucial characteristics such as corrosion resistance, resistance to thermal creep deformation and elevated temperatures strength (Zickler et al., 2009). Zinc and aluminium are essential components for chemical stability and enhanced conductivity (Bounoughaz et al., 2003; Porter, 1994; Zhang, 1996). However, using only metallic additives with their continuity at grain boundaries could cause an unfavourable condition after densification for high temperature application.

* Corresponding author at: Department of Chemical, Metallurgical and Materials Engineering, Tshwane University of Technology, Pretoria West, Pretoria 0183, South Africa.
E-mail address: ajenifujae@tut.ac.za (E. Ajenifuja).
Peer review under responsibility of King Saud University.

Production and hosting by Elsevier

https://doi.org/10.1016/j.jksus.2019.01.010
1018-3647/

Several studies have described or demonstrated the incorporation of non-metallic additives as secondary phases in metal matrix composites for improved chemical and mechanical stabilities using different powder metallurgy techniques (Kondoh, 2015; Joshi et al., 2005; Liu et al., 2006; Cui et al., 2005; Songmene and Balazinski, 1999). Ceramic secondary phases are often desired to improve sinterability and functionality of metal matrix composites (Khan and Dixit, 2017; Saheb et al., 2012). Silicon carbide has been used as additive to enhance the mechanical, thermal stability, and oxidation resistance of the nickel alloy (Saheb et al., 2012; Tjong and Ma, 2000). To the best of our knowledge, there are scarce reports on Ni alloy-ceramic composites and the contributions of SiC additives to its chemical and physical properties. Herein, we describe the preparation of nickel-based alloy reinforced with SiC particles using spark plasma sintering technique and investigate the effect of silicon carbide particle additions on the composition, microstructure, porosity, density and microhardness of Ni-base metal-ceramic matrix composites for potential use as interconnects.

2. Materials and methods

2.1. Materials and sintering procedure

Nickel, zinc, aluminium and silicon carbide powders of the desired stoichiometry of (90 − x) Ni-7Zn-3Al-*x*SiC, where x is varied from 1 to 4 were mixed in a tubular mixer at room temperature for 5 h at the rotating speed of 49 RPM. Spark plasma sintering system (l HHPD-25, FCT Germany), was employed to sinter the mixed powders at a temperature of 850 °C with heating rate of 100 °C/min, holding time of 10 min and a pressure of 50 MPa. Metal matrix composite samples of 40 mm diameter and 5 mm thickness were prepared. The sintered samples were sand blasted to completely remove the graphite foil. Summary of the procedural parameters is given in Table 1. Hence samples were polished to mirror surface for further characterizations. First, grinding was performed in two stages, using Aka-Piatto 220 and lubricating with water at the speed of 300 rpm and a force of 35 N, then using Aka-Allegran 3. The lubricant used was DiaMaxx 6 μm Poly, with speed and force of 35 N and 150 RPM respectively, for 5 min. The final polishing was performed using Aka-Napal and lubricated with DiaMaxx 1 μm Poly at 150 rpm with the force of 30 N for 4 min. The relative densities of the sintered samples were measured using Archimedes principles.

2.2. Characterization details

A precision cutting machine (BRILLANT 200) was used to cut sintered metal-ceramic composite samples to the required sizes for optical microscope examinations and the surfaces were polished with Struers polishing machine (Tegrapol-11). Following standard procedures for hard alloys, the samples were mechanically ground and polished to mirror surface using the procedure described in Section 2.1. The samples surfaces were etched with Kroll reagent for 1 min before optical microscopy examination. Scanning electron microscope (FE-SEM, JSM-7600F, JEOL Japan) and optical microscope (Nikon ECLIPSE DS-Fi1) were used for the microstructural analyses, while energy-dispersive X-ray spectroscopy (EDX) was used (integrated with FE-SEM) for compositional analysis. X-ray diffractometer (PW1710 Philips) with Cu Kα radiation at 40 kV and 40 mA was used for phase identification and chemical analysis. The diffractometry data obtained were analyzed using PANalytical X'Pert High Score software. Vickers microhardness test was performed by using Future-tech 700 microhardness tester at an indent load 100 gf, and dwelling time of 10 s.

Table 1
Sintering parameters and sintered relative densities of TiNi/CSP composites.

SPS Parameters	Values
Sintering temperature (°C)	850
Sintering pressure (MPa)	50
Chamber pressure (mbar)	5×10^{-2}
Heating rate (°C/minute)	100
Holding time (minute)	10
Maximum sintered sample density (%)	96.53
Sample thickness (mm)	5
Diameter (mm)	40

3. Results and discussions

3.1. Composition and microstructural analyses

Phase analyses of the sintered samples were done with EDX, and the identified phases are presented in Table 2, in term of their elemental concentrations. For each sample, three main phases were clearly identified (Figs. 1–4). Expectedly, all phases distinguished in the samples has nickel in combination with silicon, carbon and oxygen in substantial concentrations. With nickel as the base component, it is not unexpected for it to be significant in all phases, either as carbide or as solid solution with other metallic components. Besides nickel, carbides are also present in all observed phases. Studies have shown that apart from characteristic mechanical influence of silicon carbide additions in the matrix, i.e. grain growth inhibition and pinning (Asl et al., 2017), SiC also improved the sinterability of metal matric composites by removing the oxide impurity layer, and by forming a glassy SiO_2 phase during the sintering process (Janney, 1987; Zhang et al., 1995; Kang et al., 2005; Jaroszewicz and Michalski, 2006; Torizuka et al., 1995). In this work, formation of phases containing substantial amounts of silicon oxide are observed as highlighted in Table 1. Zinc and aluminium concentrations were found, but not in all phases, and it should be noted that both Zn and Al would be unstable at the sintering temperature, which exceeded their melting points (419.53 and 660.3 °C respectively) and there would have been a thermal reaction and transformation with nickel and SiC additive. At low SiC addition, oxidation of Zn and Al within the matrix was favoured, thereby encourage the formation of more oxides impurity layers to the detriment of the metal alloy (Figs. 1 and 2), but with relatively more SiC additions (i.e. NZAl-3SiC and NZAl-4SiC), the sinterability was remarkably improved by the removal of the oxide impurity layers and consequently forming amorphous SiO_2 phase in the sintered alloy as observed in Figs. 3 and 4 (Baik and Becher, 1987). The three main phases identified are Ni-rich, Si-C rich and C-rich. Ni-rich is characterized by smooth and uniform morphology (**B**, **F**, **G**, and **J**), as shown in the photomicrograph, it is consisted of connected polygonal grains. The representative Si-C rich phases are identified with **C**, **H**, **K** and **L**. EDX analysis also indicated formations of carbides phases with other elemental powders in the matrix.

The sample photomicrographs gave vital information about the porosity of the sintered metal composite based on SiC additions, and two distinct morphologies are markedly observed. Dark spots represented the closed pores and were dispersed within the densely packed cubic nickel-rich crystallites phases. From microstructural analyses of the phases, it is inferred that the dark porous spots observed are mostly due to direct sintering and reactions of elemental particles of zinc and aluminium within the matrix (Junior et al., 2016). However, with more SiC in the system, the porosity of the samples reduced drastically, which indicated more binary and ternary carbides formations (Figs. 3 and 4).

Table 2
Elemental characterizations of observed distinct phases in sintered metal composites.

Phase	Elements (wt%)							
	Ni	Al	Zn	Si	C	O	Cl	Fe
A	9.05	1.89	0.86	5.01	38.58	41.59	3.03	–
B	74.35	3.02	6.53	2.20	8.00	5.15	0.75	–
C	1.10	–	–	55.07	41.64	2.18	–	–
D	6.17	–	0.21	2.38	80.55	10.59	0.11	–
E	27.68	15.15	–	28.53	14.50	13.22	0.56	–
F	85.71	–	4.08	–	8.77	–	–	–
G	80.10	–	–	–	19.90	–	–	–
H	24.64	12.60	–	24.15	24.20	13.72	0.42	0.27
I	49.67	32.89	–	–	7.58	8.46	0.62	0.79
J	61.22	32.52	–	–	4.87	1.39	–	–
K	76.16	4.07	6.86	3.73	6.91	2.27	–	–
L	65.48	–	–	16.65	17.88	–	–	–

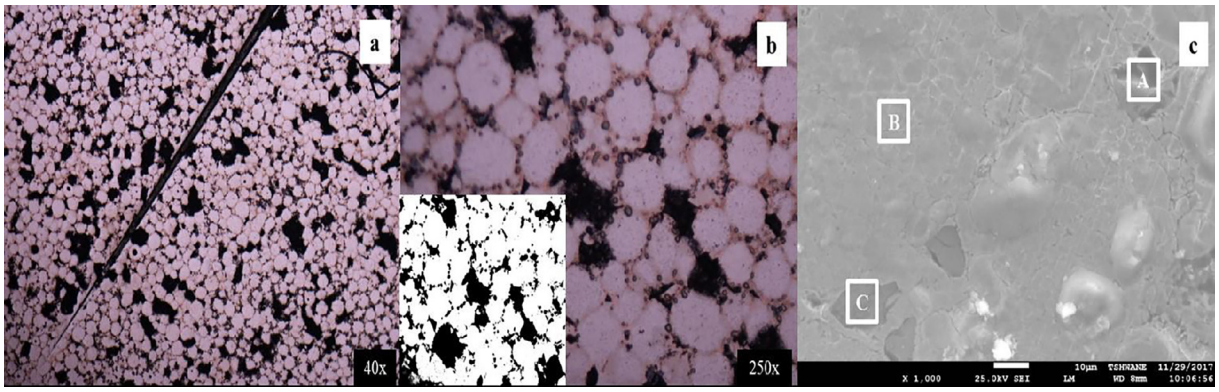

Fig. 1. Images of NZA-1SiC (a) photomicrograph 40X, (b) photomicrograph 250X, (c) SEM micrograph.

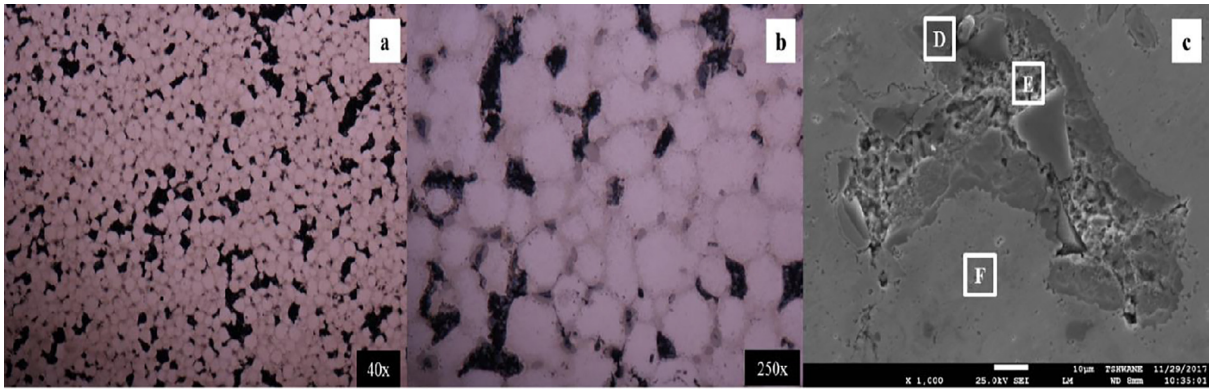

Fig. 2. Images of NZA-2SiC (a) photomicrograph 40X, (b) photomicrograph 250X, (c) SEM micrograph.

3.2. Crystallographic analysis

The diffraction patterns of the sintered samples at different SiC additions are presented in Fig. 5. The spectra obtained showed that the samples are polycrystalline in nature with sharp and distinct peaks. As indicated, the peaks are indexed to the cubic structure of nickel (Ni_4), according to the reference standards (Wyckoff, 1963; Lundqvist, 1947). The observed peaks are identical for the samples, and the peaks have preferred orientation at the planes observed at (1 1 1), (0 0 2) and (0 2 2). Direct observation of the existence of different phases could not be confirmed by the diffraction analysis, which is either due to the detection limit of the equipment or the crystallinity level of the constituent phases in the sintered metal-ceramic composite. Diffraction peaks will only emanate from phases having ordered atomic arrangement, and constructive reflections from their planes. This shows that only detectable crystalline phases of the samples consist of cubic nickel solid solution which were observed from three different 2 theta angles, and with the most preferred orientation at plane (1 1 1). This can be attributed to the concentration of the nickel in the matrix being the base metal. The increase in intensity of the diffraction lines showed that despite the reduction in weight percentage of the nickel in the metal matrix as SiC increased, there was an increase in crystallinity of the sintered metal matrix composite. It shows that the atomic arrangement of Ni-rich phases in the alloy became more orderly with SiC. These results are consistent with microhardness studies, which showed the improved hardness of the material on the addition of SiC.

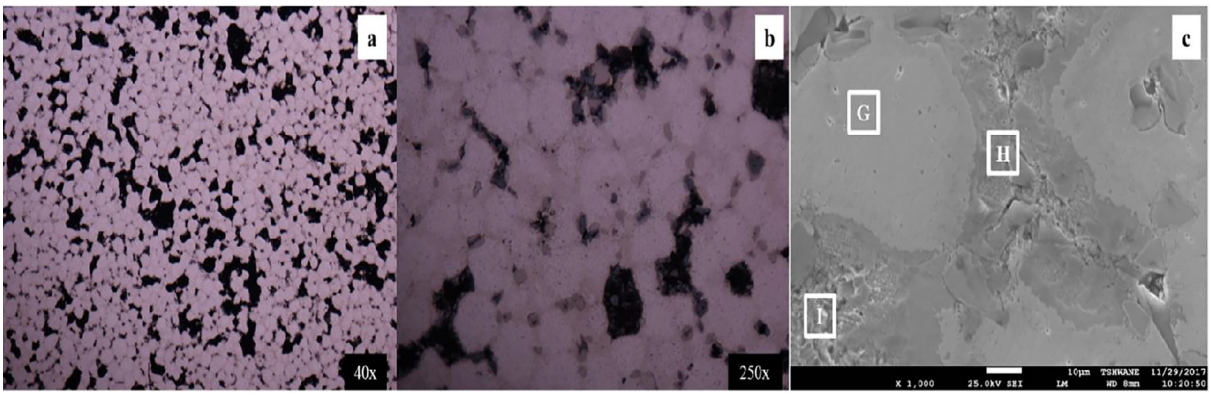

Fig. 3. Images of NZA-3SiC (a) photomicrograph 40X, (b) photomicrograph 250X, (c) SEM micrograph.

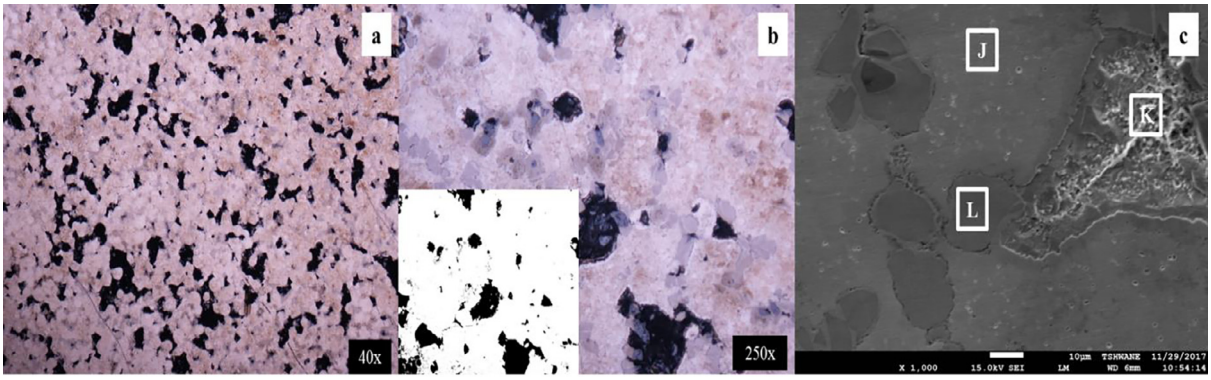

Fig. 4. Images of NZA-4SiC (a) photomicrograph 40X, (b) photomicrograph 250X, (c) SEM micrograph.

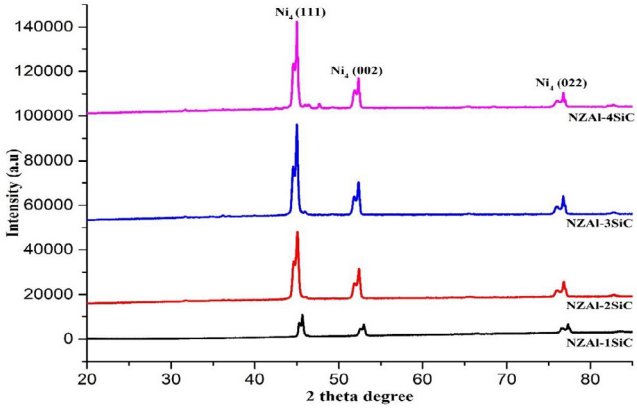

Fig. 5. XRD diffraction for samples.

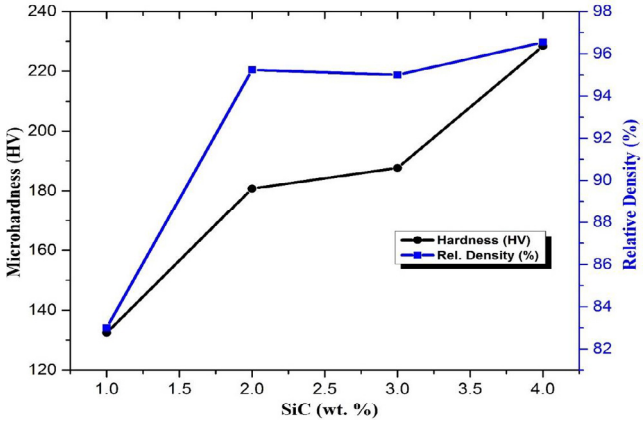

Fig. 6. Effect of SiC addition on physical properties of sintered Ni-Zn-Al-SiC.

3.3. Densification and microhardness

Density is the key factor that affects the mechanical properties of metallic alloys. Higher density alloys and metal composites generate improved mechanical properties, and additive materials can directly affect mechanical properties and densification (Asl et al., 2017). The relationships between SiC addition, density and hardness is shown in Fig. 6. The highest relative density of 96.53% was obtained at 4% SiC. As illustrated in the graphical plot, with other parameters kept constant, densification gradually increases with increasing SiC addition. Expectedly, the hardness of sample shares the same characteristic relationship with the relative density as a function of SiC. It should be noted that for pure nickel, the hardness value 65.06 HV. It is thus indicated that the higher the amount of SiC in the composite, the higher the hardness value obtained. At minimum SiC addition (NZAl-1SiC), the hardness is 132.44 HV, while 228.36 HV was obtained for sample NZAl-4SiC. From the phase composition analysis, it is clearly observed that the thermally stable SiC are well distributed in the sintered metallic composite both with the grains and at boundaries. It is ultimately inferred that improvement in hardness is due to SiC addition, and it can be adduced to the inhibition of grain growth between the metallic particles by pinning effect (Kondoh, 2015), reaction with oxide layers on metallic surfaces to form SiO_2 and formation carbide phases with elemental constituents. The direct relationship between the densification and hardness of the sintered metal-ceramic composite is also shown in Fig. 7, which is

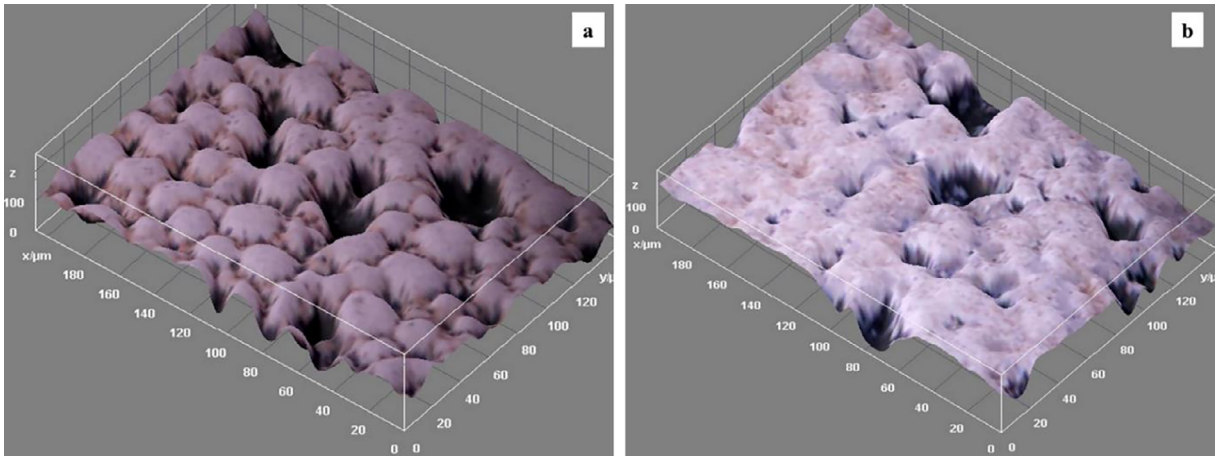

Fig. 7. Representative 3-D surface morphology images (a) NZAl-1SiC, (b) NZAl-4SiC.

the 3-D representation of morphology of sample 1 wt% SiC (Fig. 7a) and 4 wt% SiC (Fig. 7b). It is seen that sample with less porosity exhibited the highest hardness.

4. Conclusions

Silicon carbide reinforced Ni-Zn-Al metal matrix composites have been prepared using spark plasma sintering technique and based on the parameters earlier stated. The effect of additions of SiC on compositional and physical characteristics of the sintered MMC has been studied. The compositional results showed that SiC addition enhanced the formation of carbides phases with other components in the sintered specimen and SiO_2, which greatly enhanced the physical property of the system. Also, microstructural study indicated decreased in porosity, enhanced density by SiC addition, thus increase in density corresponds to increase in SiC content in the system. Hardness property of the MMC was found to be improved remarkably with the addition of SiC. Based on the present study, the optimal concentration of SiC in Ni-Zn-Al system with the best result is 4 wt%. It can be concluded that, SiC is a promising additive material to be used in the development of new fuel cell interconnect materials with enhanced physical characteristics.

Acknowledgements

The authors wish to thank Tshwane University of Technology (TUT), Pretoria, South Africa., for the supports provided during this work. Also, the support of the National Research Foundation (NRF), South Africa is hereby acknowledged.

Conflict of interest declaration

Authors declare no conflict of interest.

References

Asl, M.S., Ahmadi, Z., Parvizi, S., Balak, Z., Farahbakhsh, I., 2017. Contribution of SiC particle size and spark plasma sintering conditions on grain growth and hardness of TiB_2 composites. Ceram. Int. 43, 13924–13931.

Baik, S., Becher, P.F., 1987. Effect of oxygen contamination of densification of TiB_2. J. Am. Ceram. Soc. 70, 527–530.

Borkar, T., Banerjee, R., 2014. Influence of spark plasma sintering (SPS) processing parameters on microstructure and mechanical properties of nickel. Mater. Sci. Eng., A 618, 176–181.

Bounoughaz, M., Salhi, E., Benzine, K., Ghali, E., Dalard, F., 2003. A comparative study of the electrochemical behaviour of Algerian zinc and a zinc from a commercial sacrificial anode. J. Mater. Sci. 38 (6), 1139–1145.

Charpentier, P., 2000. Preparation of thin film SOFCs working at reduced temperature. Solid State Ionics 135 (1–4), 373–380.

Cui, Z.D., Zhu, S.L., Man, H.C., Yang, X.J., 2005. Microstructure and wear performance of gradient Ti/TiN metal matrix composite coating synthesized using a gas nitriding technology. Surf. Coat. Technol. 190, 309–313.

Folgner, C., 2017. Interconnect corrosion in steam containing fuel gas. SOFC-XV: 15th International Symposium on Solid Oxide Fuel Cells.

Janney, M.A., 1987. Mechanical properties and oxidation behaviour of a hot-pressed SiC-15 vol%-TiB2 composite. Am. Ceram. Soc. Bull. 66, 322–324.

Jaroszewicz, J., Michalski, A., 2006. Preparation of a TiB2 composite with a nickel matrix by pulse plasma sintering with combustion synthesis. J. Eur. Ceram. Soc. 26, 2427–2430.

Joshi, P.B., Marathe, G.R., Murti, N.S., Kaushik, V.K., Ramakrishnan, P., 2005. Reactive synthesis of titanium matrix composite powders. Mater. Lett. 56, 322–328.

Junior, L.A., Tomaz, Í.V., Oliveira, M.P., Simão, L., Monteiro, S.N., 2016. Development and evaluation of TiB2–AlN ceramic composites sintered by spark plasma. Ceram. Int. 40, 18718–18723.

Kang, Y.S., Kang, S.H., Kim, D.J., 2005. Effect of addition of Cr on the sintering of TiB2 ceramics. J. Mater. Sci. 40 (15), 4153–4155.

Khan, M.M., Dixit, G., 2017. Abrasive wear characteristics of silicon carbide particle reinforced zinc based composite. Silicon, 1–13.

Kondoh, K., 2015. Titanium metal matrix composites by powder metallurgy (PM) routes. In: Titanium Powder Metallurgy. Elsevier Inc., Osaka, Japan. https://doi.org/10.1016/B978-0-12-800054-0.00016-2.

Linderoth, S., 1996. Controlled reactions between chromia and coating on alloy surface. Surf. Coat. Technol. 80, 185–189.

Liu, Y., Chen, L.F., Tang, H.P., Liu, C.T., Liu, B., Huang, B.Y., 2006. Design of powder metallurgy titanium alloys and composites. Mater. Sci. Eng. A 418, 25–35.

Lundqvist, D., 1947. X-ray studies on the binary system Ni-S Locality: synthetic. Arkiv for Mineralogi och Geologi 24, 1–12.

Mohanta, L., Sathyanarayan, R., Venkateswaran, K., 2014. Study of The Nickel Base Alloy For High Performance Application. Abdur Rahman University, 6(10), 1–5.

Porter, F., 1994. "Wrought Zinc". Corrosion Resistance of Zinc and Zinc Alloys. CRC Press.

Saheb, N., Iqbal, Z., Khalil, A., Hakeem, A.S., Al Aqeeli, N., Laoui, T., Al-Qutub, A., Kirchner, R., 2012. Spark plasma sintering of metals and metal matrix nanocomposites: a review. J. Nanomater. 18.

Songmene, V., Balazinski, M., 1999. Machinability of graphitic metal matrix composites as a function of reinforcing particles. CIRP Ann. Manuf. Technol. 48 (1), 77–80.

Tang, C.F., Pan, F., Qu, X.H., He, X.B., 2009. Nickel base superalloy GH4049 prepared by powder metallurgy. Alloy Compd. 474 (474), 201.

Tjong, S.C., Ma, Z.Y., 2000. Microstructural and mechanical characteristics of in situ metal matrix composites. Mater. Sci. Eng.: R: Rep. 29 (3), 49–113.

Torizuka, S., Sato, K., Nishio, H., Kishi, T., 1995. Effect of SiC on interfacial reaction and sintering mechanism of TiB2. J. Am. Ceram. Soc. 78 (6), 1606–1610.

Wachsman, E., Lee, K., 2011. Lowering the temperature of solid oxide fuel cells. Science 334, 935.

Wyckoff, R.W., 1963. Cryst. Struct. 1, 7–83.

Zeblon, M.E., Ajenifuja, E., Ajao, J.A., 2018. Thermal and microstructural study of slowly cooled Ni-B hard alloys containing Ti. J. Mater. Res Technol.

Zhang, X.G., 1996. Corrosion and Electrochemistry of Zinc. Springer.

Zhang, G.J., Jin, Z.Z., Yue, X.M., 1995. Reaction synthesis of TiB2-SiC composites from TiH2-Si-B4C. Mater. Lett. 25, 97–100.

Zickler, G.A., Schnitzer, R., Radis, R., Hochfellener, R., Scheweins, R., Stockinger, M., Leitner, H., 2009. Microstructures and mechanical properties of the super alloy ATI Allvac 718 Plus. Mater. Sci. Eng. 4, 1–9.